First implosion experiments with cryogenic thermonuclear fuel on the National Ignition Facility

2012 Plasma Phys. Control. Fusion 54 045013

(http://iopscience.iop.org/0741-3335/54/4/045013)

Plasma Phys. Control. Fusion **54** (2012) 045013 (13pp) doi:10.1088/0741-3335/54/4/045013

First implosion experiments with cryogenic thermonuclear fuel on the National Ignition Facility*

Siegfried H Glenzer[1,8], Brian K Spears[1], M John Edwards[1], Ethan T Alger[2], Richard L Berger[1], Darren L Bleuel[1], David K Bradley[1], Joseph A Caggiano[1], Debra A Callahan[1], Carlos Castro[1], Daniel T Casey[3], Christine Choate[1], Daniel S Clark[1], Charles J Cerjan[1], Gilbert W Collins[1], Eduard L Dewald[1], Jean-Michel G Di Nicola[1], Pascale Di Nicola[1], Laurent Divol[1], Shamasundar N Dixit[1], Tilo Döppner[1], Rebecca Dylla-Spears[1], Elizabeth G Dzenitis[1], James E Fair[1], Lars Johan Anders Frenje[3], M Gatu Johnson[3], E Giraldez[2], Vladimir Glebov[5], Steven M Glenn[1], Steven W Haan[1], Bruce A Hammel[1], Stephen P Hatchett II[1], Christopher A Haynam[1], Robert F Heeter[1], Glenn M Heestand[1], Hans W Herrmann[4], Damien G Hicks[1], Dean M Holunga[1], Jeffrey B Horner[1], Haibo Huang[1], Nobuhiko Izumi[1], Ogden S Jones[1], Daniel H Kalantar[1], Joseph D Kilkenny[2], Robert K Kirkwood[1], John L Kline[4], James P Knauer[5], Bernard Kozioziemski[1], Andrea L Kritcher[1], Jeremy J Kroll[1], George A Kyrala[4], Kai N LaFortune[1], Otto L Landen[1], Douglas W Larson[1], Ramon J Leeper[6], Sebastien Le Pape[1], John D Lindl[1], Tammy Ma[1], Andrew J Mackinnon[1], Andrew G MacPhee[1], Evan Mapoles[1], Patrick W McKenty[5], Nathan B Meezan[1], Pierre Michel[1], Jose L Milovich[1], John D Moody[1], Alastair S Moore[7], Mike Moran[1], Kari Ann Moreno[2], David H Munro[1], Bryan R Nathan[1], Abbas Nikroo[2], Richard E Olson[6], Charles D Orth[1], Arthur Pak[1], Pravesh K Patel[1], Tom Parham[1], Richard Petrasso[3], Joseph E Ralph[1], Hans Rinderknecht[3], Sean P Regan[5], Harry F Robey[1], J Steven Ross[1], Jay D Salmonson[1], Craig Sangster[5], Jim Sater[1], Marilyn B Schneider[1], F H Séguin[3], Michael J Shaw[1], Milton J Shoup[5], Paul T Springer[1], Wolfgang Stoeffl[1], Larry J Suter[1], Cliff Avery Thomas[1], Richard P J Town[1], Curtis Walters[1], Stephen V Weber[1], Paul J Wegner[1], Clay Widmayer[1], Pamela K Whitman[1], Klaus Widmann[1], Douglas C Wilson[4], Bruno M Van Wonterghem[1], Brian J MacGowan[1], L Jeff Atherton[1] and Edward I Moses[1]

[1] Lawrence Livermore National Laboratory, Livermore, CA 94550, USA
[2] General Atomics, San Diego, CA 92121, USA
[3] Plasma Fusion and Science Center, Massachusetts Institute of Science and Technology, Cambridge, MA 02139, USA
[4] Los Alamos National Laboratory, Los Alamos, NM 87545, USA
[5] Laboratory for Laser Energetics, University of Rochester, Rochester, NY 14623, USA
[6] Sandia National Laboratory, Sandia, NM 87185, USA
[7] Atomic Weapons Establishment, Aldermaston, RG7, UK

E-mail: glenzer1@llnl.gov

Received 24 November 2011, in final form 24 January 2012
Published 21 March 2012
Online at stacks.iop.org/PPCF/54/045013

[8] Author to whom any correspondence should be addressed.
* Part of the EPS 2011 special issue. Based on the plenary talk by S H Glenzer at the 38th EPS Plasma Physics meeting in Strassbourg, 2011.

Abstract

Non-burning thermonuclear fuel implosion experiments have been fielded on the National Ignition Facility to assess progress toward ignition by indirect drive inertial confinement fusion. These experiments use cryogenic fuel ice layers, consisting of mixtures of tritium and deuterium with large amounts of hydrogen to control the neutron yield and to allow fielding of an extensive suite of optical, x-ray and nuclear diagnostics. The thermonuclear fuel layer is contained in a spherical plastic capsule that is fielded in the center of a cylindrical gold hohlraum. Heating the hohlraum with 1.3 MJ of energy delivered by 192 laser beams produces a soft x-ray drive spectrum with a radiation temperature of 300 eV. The radiation field produces an ablation pressure of 100 Mbar which compresses the capsule to a spherical dense fuel shell that contains a hot plasma core 80 μm in diameter. The implosion core is observed with x-ray imaging diagnostics that provide size, shape, the absolute x-ray emission along with bangtime and hot plasma lifetime. Nuclear measurements provide the 14.1 MeV neutron yield from fusion of deuterium and tritium nuclei along with down-scattered neutrons at energies of 10–12 MeV due to energy loss by scattering in the dense fuel that surrounds the central hot-spot plasma. Neutron time-of-flight spectra allow the inference of the ion temperature while gamma-ray measurements provide the duration of nuclear activity. The fusion yield from deuterium–tritium reactions scales with ion temperature, which is in agreement with modeling over more than one order of magnitude to a neutron yield in excess of 10^{14} neutrons, indicating large confinement parameters on these first experiments.

(Some figures may appear in colour only in the online journal)

1. Introduction

Following commissioning of the National Ignition Facility (NIF) [1, 2] and demonstration of hohlraum symmetry [3–5] with adequate soft x-ray drive [6–8] several new experimental platforms have been fielded to study the performance of indirectly driven inertial confinement fusion capsule implosions [9, 10]. These experiments [11] measure and optimize four general parameters including symmetry during the foot and the peak of the laser drive, shock timing, implosion velocity and hydrodynamic mix. The goal of the campaigns is to field a fusion experiment that uses equimolar deuterium–tritium (DT) fill and that has a high probability for achieving ignition and burn [12, 13].

Of central importance to the progress toward ignition with each tuning step is the assessment of hot-spot formation and thermonuclear fuel assembly. These processes are characterized by the neutron yield from primary DT reactions in the central hot plasma, D + T $=$ ^{4}He(3.5 MeV) + n(14.1 MeV), and the ratio of down scattered to primary neutrons, N(10–12 MeV)/N(13–15 MeV), quantifying neutrons that have lost energy by scattering processes in the dense fuel plasma that surrounds the central hot plasma. These measured quantities are combined into an experimental ignition threshold factor [14, 15]. Radiation-hydrodynamic simulations and analytical modeling have shown that this performance metric can be tied to the Lawson confinement criterion [16] for inertial confinement fusion [17, 18] that measures the proximity of a fusion experiment toward the regime of sufficient density or pressure, confinement time and temperature required for ignition. For this purpose, cryogenic layered capsule implosion experiments have been designed to emulate ignition conditions in a non-alpha particle self-heating, non-burning implosion, thus allowing a large suite of diagnostics to be fielded in a controlled neutron flux environment [19].

The implosion experiments employ a 2.26 mm diameter fusion capsule with approximately 0.17 mg of nuclear fuel. The fuel is prepared cryogenically into a solid ice layer of hydrogen isotopes on the inside of a low-Z (plastic) ablator. The capsule is placed in the center of a centimeter-scale hohlraum that is heated by up to 1.3 MJ of laser energy, generating ablation pressures in excess of 100 Mbar. The rocket-like acceleration of the shell in response to the ablation pressure compresses the shell toward the center with the goal to produce fuel densities of 1000 g cm^{-3}. This high density shell of fuel surrounds a hot spot which, for ignition, will reach temperatures in excess of 10 keV from a combination of PdV work and alpha particle deposition. At this point, a nuclear burn wave is launched igniting the surrounding dense fuel, sustained by alpha particle deposition and electron conduction without an external energy source [9, 10, 20, 21]. Burning approximately 1/3 of the DT-fuel will result into 6.5×10^{18} fusion neutrons with a total neutron yield of 15 MJ.

In this study, the fuel has been diluted using tritium–hydrogen–deuterium (THD) mixtures; specifically 6% deuterium to control nuclear yield, and 72% tritium with 22% hydrogen to provide the same fuel mass as in DT implosions. The fuel has been fielded in a 68 μm thick layer. A fuel layer with characteristics that meets the specifications for ignition has been demonstrated, i.e. adequate sphericity with a total groove area from local defects of less than 200 μm^2 and an averaged root mean square value of less than 0.7 μm. The laser-driven hohlraum radiation field compresses the capsule symmetrically to a sphere with a central hot-spot diameter of 80 μm. In addition, the experiments have successfully demonstrated the control of the implosion shape using ignition grade cryogenic fuel layers [22], laser power balance and pulse shaping [2], and plasma optics gratings [3, 4, 23]. For a burn-averaged ion temperature of T_i $=$ 3.5 keV, these implosions provide 10^{14} neutrons at 14.1 MeV energy and an accurate ($\pm$10%) measurement of the

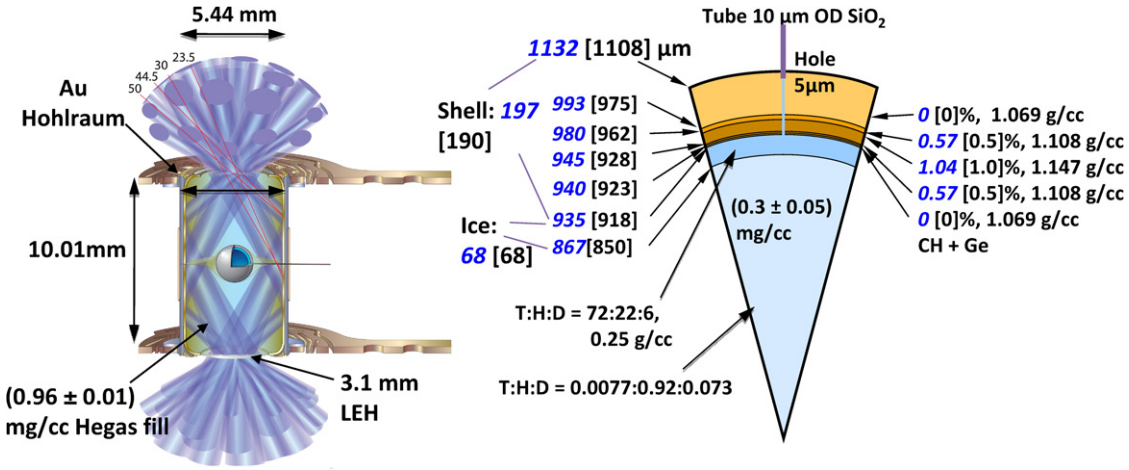

Figure 1. Schematic of an ignition scale hohlraum is shown along with a fusion capsule for cryogenic layered implosions. Numbers in black describe the specification and numbers in blue italic represent the experimental shot conditions. The hohlraum is heated with 192 laser beams in four cones at angles of 23.5°, 30°, 44.5° and 50° to the hohlraum axis. The fusion capsule uses five plastic layers of various thickness, three of which are doped with germanium with varying concentration to absorb high-energy x-rays from the gold hohlraum and to tailor the density gradient at the ablator–fuel interface. On the inside of the ablator, a 68 μm thick ice layer is produced that contains most of the nuclear fuel.

down-scattered ratio, i.e. the neutron fraction that lost energy in the dense fuel through scattering processes. These first experiments show high values for the Lawson fusion parameter and demonstrate thermonuclear fuel implosion experiments that provide adequate implosion performance data on hot-spot formation and nuclear fuel assembly needed for determining progress toward ignition.

The paper is organized as follows. Section 2 describes the hohlraum and capsule target together with fuel layer capabilities on NIF. An example of a groove analysis for a cryogenic fuel layer used for shot selection is also provided. Section 3 describes the laser drive and soft x-ray production in the hohlraum. The resulting capsule implosion symmetry and core shape is shown. Section 4 presents nuclear data from cryogenic layered implosion experiments indicating accurate measurements of hot spot formation and nuclear fuel assembly. This section also provides a brief performance assessment analysis in the form of an experimental ignition threshold factor and estimates of the Lawson confinement parameter that shows high values for these initial experiments. Section 5 presents the conclusions.

2. Cryogenic thermonuclear fuel targets

2.1. Hohlraum and capsule

Figure 1 shows a schematic of the hohlraum, capsule and nuclear fuel ice layers employed in these experiments. For a fuel layer with 6% D, the targets are prepared cryogenically to achieve a nominal shot temperature of 17.4 K, i.e. $\Delta T = -1.5$ K below the triple point of the phases of THD. This temperature is reached a few seconds before the system shot by lowering the target temperature over a period of a 30 s long quench. Active (cascade) temperature control during this time ensures that the required shot temperature is reached with an uncertainty smaller than 2 mK.

The quench is implemented to provide the desired vapor pressure inside the fusion capsule with a gas density of 0.3 mg for DT [24]. This procedure is required because smooth ice layer surfaces can currently be made only close to the triple point [22]. Independent tests have shown that the layer quality is stable from the time-of-final layer characterization to the laser shot. At cryogenic temperatures the gold hohlraums are 1 cm long with a diameter of 5.44 mm and filled with helium gas at a pressure of 260 torr resulting in densities of 0.96 mg cm^{-3}.

Figure 2 shows two views of an ignition hohlraum target mounted on the cryogenic target positioner before being enclosed by a shroud. The shroud protects the target from chamber thermal radiation during the cryogenic layering process as well as from gaseous impurities that condenses on cold surfaces. The shroud opens 8 s before the laser beams are fired; the opening results in an increase in temperature due to exposure to thermal radiation of about 400 mK, which is compensated for so that the final temperature is reached within less than 3 s. Protection of the target from ice condensates during layering and during the final exposure to the target chamber atmosphere is provided by the laser entrance hole (LEH) storm windows. These consist of thin plastic foils coated with 40 nm carbon film to absorb 100 K and 300 K thermal radiation which will keep the LEH ice free. This important feature has enabled proper laser beam propagation during the low power foot of the laser pulse at a typical chamber pressure of 10^{-5} torr and a total exposure of 2.3×10^{-4} torr h. Thus, the first shock launched during the early time laser picket of an ignition laser pulse is adequately delivered [25]. In this study, we show that when storm windows are used, there is an approximate agreement in the observed implosion symmetry of a layered THD implosions and high-pressure gas-filled plastic shells, i.e. symcap implosions.

2.2. Thermonuclear fuel layer

Figure 3 shows characterization of the fuel distribution inside the capsule measured along 3 lines of sight with 9 keV x-ray

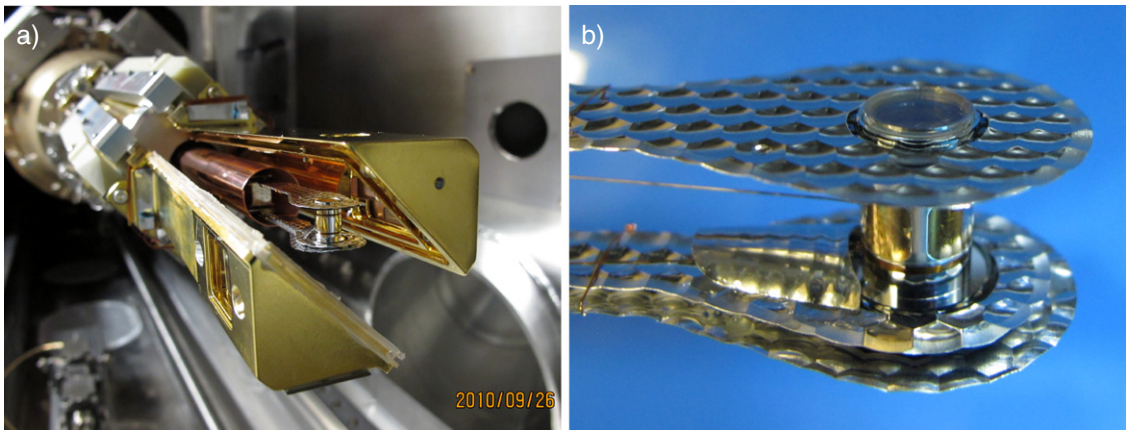

Figure 2. (*a*) Picture of cryogenic ignition target before fully enclosed by the shroud. (*b*) The storm window is seen on the top laser entrance hole (LEH) of the cylindrical hohlraum target. On the side of the hohlraum, a cutout can be identified which is covered with a 10 nm thick Au coating and that allows characterization of the ice fuel layer during the layering process.

point projection radiography using a tungsten L-emission source. An axial view (figure 3(*a*)) is provided through the LEHs and 2 orthogonal views (figures 3(*b*) and (*c*)) are obtained in the equatorial plane through cut outs in the hohlraum cylinder walls. These so-called starburst windows can be identified underneath a 10 μm gold coating in figure 2 on the side of the hohlraum.

Ice layer preparation is performed within a shroud that consists of two enclosures; the outer one at 300 K and the inner one cooled to 100 K. The shroud has 4 Al-coated and 12 Au-coated windows to allow x-ray characterization and subsequent alignment of the target at target chamber center. These alignment windows are covered with a total of 25 nm thick gold foils to prevent thermal radiation from heating the target. The capsule is first filled at a temperature of 500 mK below the triple point of the THD fill so that the fuel is in a slightly supercooled liquid state. Filling will continue until the height of the meniscus as observed in the side windows approximately indicates the desired fuel inventory, see figure 3(*d*). The target is then cooled rapidly by 1–2 K to plug the fill tube and to obtain the total capsule fuel.

The resulting ice is polycrystalline with many crystals. A subsequent slow warming period of the capsule, at a rate of 1 mK min^{-1} to 18.9 K ($\pm$0.03 K) for THD or 19.8 K ($\pm$0.03 K) for DT, will melt the solid back into the fill tube. The ice will melt and accumulate at the bottom of the capsule; the meniscus height will increase until the maximum of the triple point range has been reached; for THD this range may approach 100 mK and for DT the range is 30 mK. With frozen ice in the fill tube isolating the capsule from the reservoir, a measurement of the meniscus height of 258 μm ($\pm$4.5 μm) determines the final fuel inventory. Figure 3(*d*) shows the fill that provides an ice layer thickness of 68 μm $\pm$1.5 μm.

A subsequent drop in the capsule temperature by 45 mK is performed so that the fill tube ice provides a seed for growing the capsule ice layer with the correct orientation [22]. The seed is initially in an unstable fcc ice phase which converts to hcp crystals. Layering is started at a temperature of 100 mK below the triple point and slowly cooled to about 400 mK below the triple point over a period of 14 to 18 h. This method relies on the radioactive self-heating from beta decay in the condensed THD, which enables redistribution of the solid along the isotherms in the capsule and is known as beta layering [26–28]. The target is then shot within 3 days to prevent helium build-up from beta decay of tritium.

2.3. Fuel layer characterization

Figure 3(*e*) shows an example of the results from a mode analysis for a layered THD experiment. The power spectral density (PSD) provides a measurement of the deviation from a spherical shape along the three lines of sight for all modes starting from $m = 2$ to $m = 150$. Also shown is the NIF specification that is derived from radiation-hydrodynamic simulations [29, 30] and that estimates the maximum deviation allowed for an ignition experiment. This measurement of background roughness of ice layers is then used to calculate the effect on the observed neutron yield. For this purpose, we normalize the measured PSD to the specification and average over the four ranges of modes with different slopes,

$$nfa = \sqrt{\sum_{j=1}^{4} nf_j^2} \tag{1}$$

with

$$nf_1 = \sqrt{\frac{1}{6}\sum_{m=1}^{6}\frac{PSD_m}{PSD_{\text{spec}}}}, \quad nf_2 = \sqrt{\frac{1}{6}\sum_{m=7}^{12}\frac{PSD_m}{PSD_{\text{spec}}}},$$
$$nf_3 = \sqrt{\frac{1}{13}\sum_{m=13}^{25}\frac{PSD_m}{PSD_{\text{spec}}}}, \quad nf_4 = \sqrt{\frac{1}{125}\sum_{m=26}^{150}\frac{PSD_m}{PSD_{\text{spec}}}}. \tag{2}$$

This mode analysis is combined with an estimate for the impact of isolated defects on the neutron yield of tuned implosions. The total effect of grooves on hot-spot rms takes

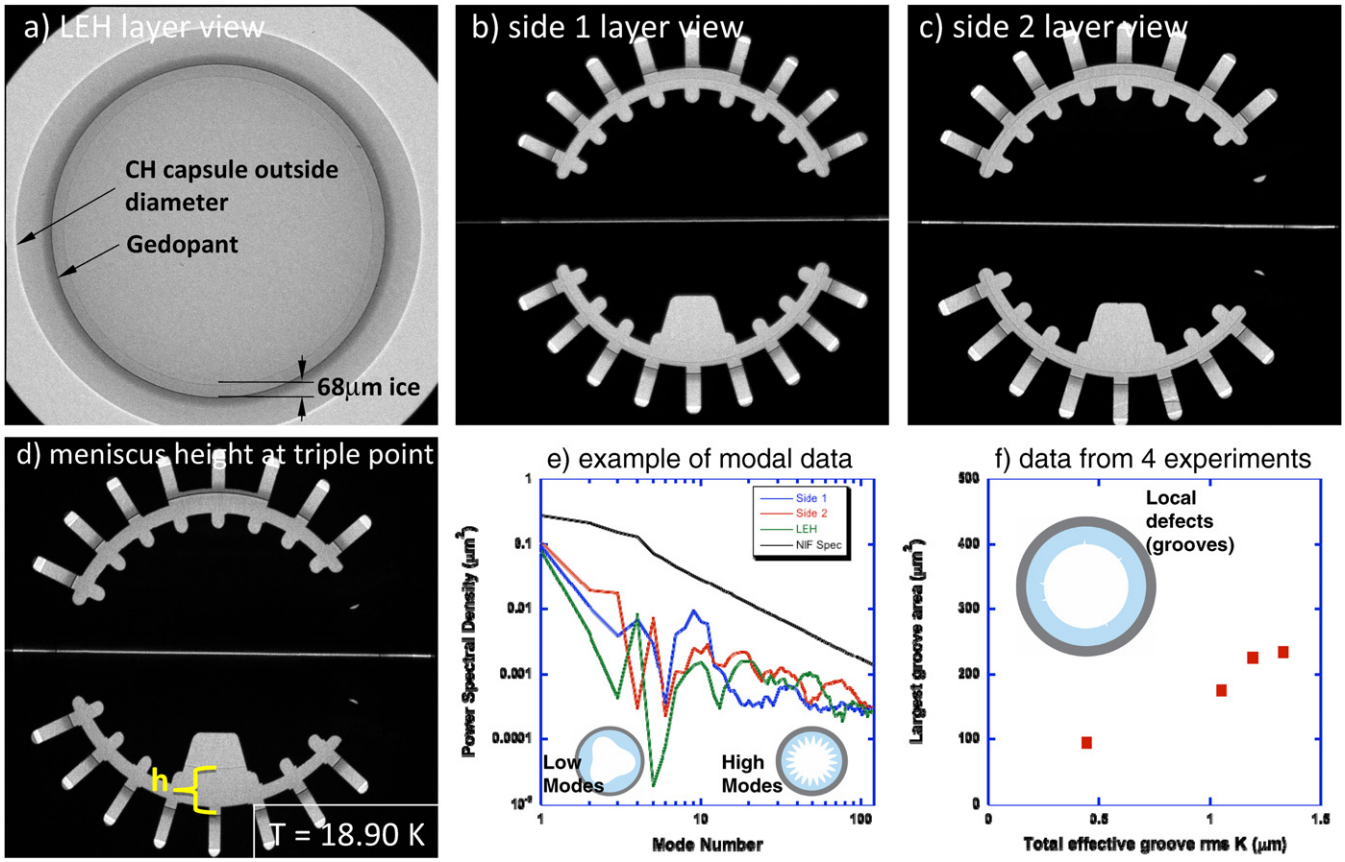

Figure 3. X-ray characterization of THD ice layers at a temperature of 18.4 K through the LEH and the star burst cut outs. (*a*)–(*c*) A fusion capsule is shown from three lines of sight. The dark ring is due to absorption of x-rays in the Ge-doped plastic shell and a 68 μm-thick THD ice layer can be seen on the inside of the shell. Also shown (*d*) is the capsule with THD fill at the triple point temperature of 18.9 K. The power spectral density versus mode number is shown in (*e*). A summary of the layer groove characterization is provided in terms of the maximum length and the K-values for the first four THD shots (*f*).

into account the sum over all defects of area A and length L,

$$K = \sqrt{\frac{1}{V_{\text{fuel}}} \sum_{j=1}^{n} A_j^2 L_j}, \tag{3}$$

where we require

$$A \leqslant 250\,\mu\text{m}^2 \tag{4}$$

to avoid a groove from breaking through the DT layer during the implosion.

Figure 3(*f*) shows the largest groove area and the effective K-values for four implosion experiments. These data show one ignition grade layer with $K < 0.7$ and three marginal layers for tuning experiments, $0.7 < K < 1.5$. The effect of non-perfect layers on the neutron yield is estimated

$$\text{yf} = 1.3 - \frac{3}{\sqrt{2}} \left(4.9 \times 10^{-3} n f a^2 + 1 \times 10^{-1} K^2\right)^{\frac{1}{2}}. \tag{5}$$

We find a yield factor of yf $= 1$ for the ignition grade layer with $A < 100\,\mu\text{m}^2$, $K < 0.5\,\mu$m; for the remaining three layers these values reduce to yf $= 0.5 \pm 0.1$. The calculated neutron yield performance will be lowered by including the effects of ice roughness on the capsule. The yield factor will likely be improved and approach a value of yf $\simeq 1$ in future layered experiments as tests have shown improved layer quality with increasing deuterium fraction.

3. Capsule implosion experiments

3.1. Laser drive

The hohlraums are heated with 192 frequency-tripled (3ω) laser beams at a wavelength of 351 nm through two LEHs of 3.1 mm diameter on either end, cf figure 1. The beams are arranged in four cones entering through each LEH; the inner two cones being at angles of 23.5° and 30° and the outer two cones being at 44.5° and 50° to the vertical axis.

Figure 4(*a*) shows examples of the total 3ω laser powers together with the powers in the inner and outer cones of beams. In these experiments, the laser beams delivered up to 400 TW peak power in a 21 ns long shaped pulse, providing a total energy of (1.3 ± 0.03) MJ energy. We employ smoothed beams [2, 31, 32] with polarization rotation [33, 34], smoothing by spectral dispersion with a laser bandwidth of 60 GHz and a 17 GHz frequency oscillator. In addition, continuous phase plates are employed that give elliptical vacuum spot sizes [35, 36] major radius, a, and minor radius, b, of the ellipse. On the 23.5° beams we use $a = 0.8817$ mm, $b = 0.6313$ mm, on the 30° beams we use $a = 0.824$ mm, $b = 0.59$ mm, on the 44.5° beams we use $a = 0.6345$ mm, $b = 0.6313$ mm, and on the 50° beams we use $a = 0.593$ mm, $b = 0.343$ mm. These spots result in quad vacuum peak intensities

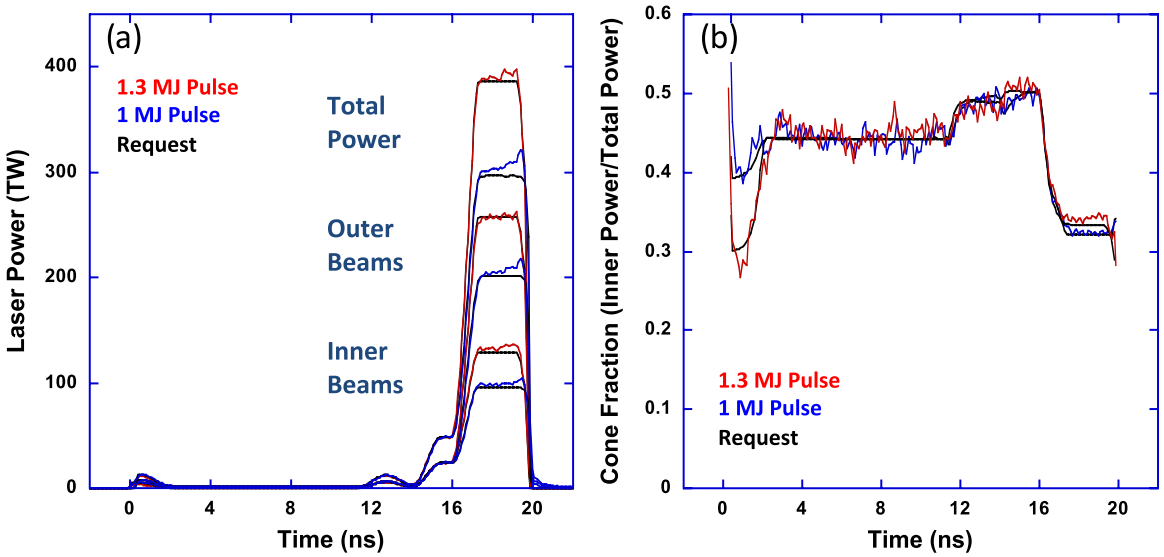

Figure 4. (*a*) Measured incident and requested laser powers of hohlraums driven by total energies of 1 MJ (blue) and 1.3 MJ (red) for shots N100929 and N110212, respectively. The total laser powers are shown together with power on the outer and inner cones of beams. While the 1 MJ laser pulse reaches a peak power of 300 TW, the 1.3 MJ drive rises to 400 TW with a 600 ps faster rise. (*b*) The laser cone fractions as a function of time are shown; the 1.3 MJ laser drive employs a lower equatorial drive during the early picket (0–2 ns) and a slightly higher equatorial drive at peak power (17–20 ns).

of $I_{23.5} = 4.8 \times 10^{14}\,\mathrm{W\,cm^{-2}}$, $I_{30} = 5.5 \times 10^{14}\,\mathrm{W\,cm^{-2}}$, $I_{44.5} = 1.2 \times 10^{15}\,\mathrm{cm^{-2}}$ and $I_{50} = 1.3 \times 10^{15}\,\mathrm{W\,cm^{-2}}$ for the 400 TW laser drive.

For the NIF hohlraum and laser configuration, a total of 64 inner beams (16 quads) are focused into a ring in the equatorial plane of the hohlraum, 8 quads from the top hemisphere in the 23.5° and 30° cones and 8 quads from the bottom hemisphere. In addition, on either side of the capsule, 16 outer quads irradiate the hohlraum wall in a ring-like pattern about half way between the equatorial plane and the LEH plane, see figure 1. Thus, we expect a symmetric capsule implosion when the beam power in the three rings of beams is balanced such that the inner beam power is approximately 1/3 of the total power. At the peak of the drive, this choice for the laser cone fractions was adopted while the early picket cone fraction has been adjusted between the 1 MJ and 1.3 MJ implosions based on improved symmetry information from re-emit experiments [37], see figure 4(*b*). In this study, calculations have determined the cone fraction during the remaining parts of the laser pulse. In future tuning experiments, symmetry will be tuned throughout the pulse using velocity interferometer measurements on the shock waves at two orthogonal angles [38–40].

At these energies and powers, the hohlraum absorbs 80–90% of the incident energy with the dominating loss mechanism being due to stimulated Raman scattering (SRS) [41, 42] on the inner cones of beams as measured with a full aperture backscatter diagnostics and near backscatter imagers [43]. For example, the 1.3 MJ driven hohlraum shows a total of 14.2 kJ[±4.3 kJ] on a 23.5° quad of beams and 12.7 kJ[±3.9 kJ] on a 30° quad of beams. Scattering losses on the outer beams are negligible, a total of 210 J [±40 J] of stimulated Brillouin scattering has been measured on a 50° quad of beams. With 8 quads at 23.5° and 8 quads at 30° relative to the hohlraum axis, these measurements result in an estimated coupling of $1 - [222\,\mathrm{kJ}/1300\,\mathrm{kJ}] = 0.83 \pm 0.04$ providing 1.08 MJ of absorbed laser energy to achieve the required radiation temperature and to drive the implosion.

SRS can effect the implosion performance in two important ways. First, damping of the SRS-driven electron plasma waves produces hot electrons [44, 45]. Measurements with an x-ray filter fluorescer [46] indicate about 500 J of electrons with energies >170 keV that have the potential to generate capsule preheat. The measured hot electron numbers are about a factor of 2 below current tolerated upper limits for ignition [7, 9]. Direct hard x-ray imaging of the capsule implosion has recently shown that preheat of the fuel is consistent with the low estimate by FFLEX [47]. Secondly, SRS losses affect capsule implosion symmetry.

In this study, the SRS scattering losses on the inner beams have been compensated for and a symmetric radiation drive on the capsule has been achieved using laser wavelengths of 1053.4 nm on the 23.5° and 30° cones of beams and 1052.8 nm on the 44.5° and 50° cones of beams. The wavelength shift enhances power transfer from the outer cones of laser beams to the inner cones by laser scattering on self-generated plasma optics gratings in the LEH area [3, 4, 23, 48, 49]. Power transfer increases the inner beam power by a factor of $1.5 - 2$ while allowing all beams to be operated at maximum power producing the required symmetric soft x-ray drive on the capsule (section 3.3).

3.2. Hohlraum temperature

Figure 5 shows experimental and calculated hohlraum radiant intensity as a function of time. The measurements of the x-ray power, P, in the energy range $0 < E_{\text{x-ray}} < 20$ keV out of the LEH, have been performed with the absolutely calibrated broadband x-ray spectrometer Dante [6, 50, 51]. We find that both the temporal dependence and peak values are in excellent

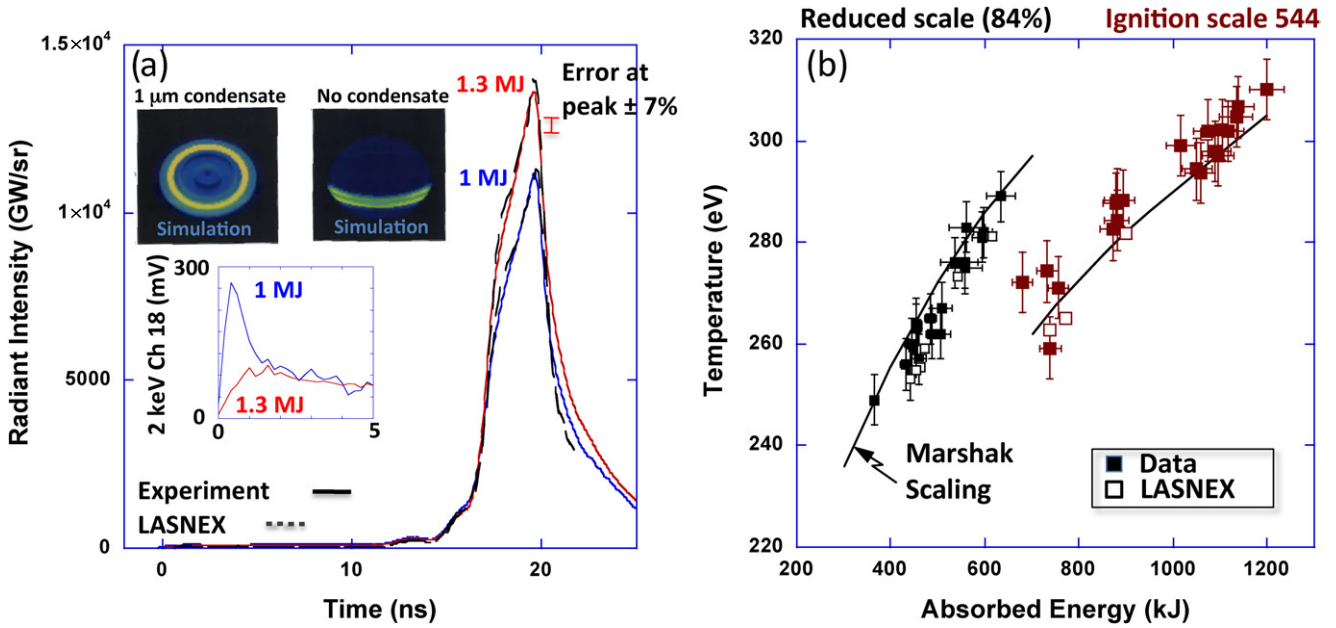

Figure 5. (*a*) Measured and calculated (*a*) Dante hohlraum radiant intensity as function of time for 1 MJ N100929 shot and 1.3 MJ N110212 shot. The inset in (*a*) shows 2 keV Dante channel 18 and calculated Dante images during the first 2 ns. (*b*) Hohlraum peak radiation temperatures are shown versus absorbed laser energy.

agreement with radiation-hydrodynamic modeling using the code LASNEX [8, 29]. Also shown as insets are the voltage traces from Dante channel 18, which has been set up to observe Ar K-shell x-rays at 2 keV along with simulated total soft x-ray Dante images at 2 ns into the pulse.

From the measured radiant intensity, the temperature can be inferred via $\mathrm{d}P/\mathrm{d}\Omega = A_{\mathrm{LEH}}(t)\phi(t)\cos\theta\sigma T_{\mathrm{RAD}}^4/\pi$. Here, σ is the Stefan–Boltzmann constant and θ is the view angle of Dante toward the hohlraum axis. The dynamically varying source area, $A_{\mathrm{LEH}}(t)$, is estimated from the 3–5 keV x-ray images [52] of the LEH measured with the static x-ray imager, SXI, see figure 1. These measurements show a reduction of the LEH diameter to 83% of the initial value. ϕ is the view factor that relates the Dante measured drive with the radiation temperature seen by the capsule.

Recent implementation of a time-integrating soft x-ray imager of the LEH at 900 eV has provided new measurements of the LEH aperture, indicating that about 10% of the Dante measured radiant intensity is due to emission from the ablated Au plasma that reduces the LEH clear aperture [53]. Assuming 90% of the measured flux from the hohlraum interior, applying the measured LEH aperture, and adding a small view-factor correction results in 10 eV corrections for these experiments.

The internal hohlraum radiation temperatures are modeled by balancing the absorbed laser power with the x-ray power radiated into the wall, P_{W}, absorbed by the capsule, P_{CAP}, and the power that escapes through the LEH, P_{LEH},

$$\eta_{\mathrm{CE}}\,(P_{\mathrm{L}} - P_{\mathrm{Backscatter}}) = P_{\mathrm{W}} + P_{\mathrm{LEH}} + P_{\mathrm{CAP}}$$
$$= \sigma T_{\mathrm{RAD}}^4\,[(1-\alpha_{\mathrm{W}})A_{\mathrm{W}} + A_{\mathrm{LEH}} + (1-\alpha_{\mathrm{CAP}})A_{\mathrm{CAP}}]\,. \quad (6)$$

With η_{ce} being the x-ray conversion efficiency from laser power to soft x-rays [54]; α_{W} and α_{CAP} are the x-ray albedo of the hohlraum wall and the capsule, respectively. The albedo is defined as the ratio of re-emitted to incident x-rays. The hohlraum wall area, LEH area, and capsule surface area are denoted by A_{W}, A_{LEH} and A_{CAP}, respectively. Assuming a conversion efficiency of $\eta_{\mathrm{CE}} = 0.9$ at peak laser power, equation (6) indicates peak radiation temperatures of 260 eV $< T_{\mathrm{RAD}} <$ 305 eV for experiments with varying peak laser power.

Figure 5(*b*) shows the experimental peak radiation temperatures for various hohlraum experiments as a function of the absorbed energy along with results from radiation-hydrodynamic modeling with the code LASNEX that uses the detailed configuration accounting model for x-ray opacities [8]. Generally, we observe good agreement between data and modeling; in particular, at ignition scale we have achieved a hohlraum drive of 300 eV at 1.1 MJ absorbed energy. Also shown in figure 5 are the Marshak scaling results [55–57] of equation (6) assuming a conversion efficiency of $\eta_{\mathrm{ce}} = 0.9$ and the albedo calculated according to [58]. The latter increases according to the data and integrated modeling and provides a good match to the experimental data at both hohlraum scales.

The uncertainty of the measured radiant intensity is 7%, which results in an error bar of ±5 eV for the measured peak radiation temperature. In this study, the analysis does not include the very soft channels of Dante that are contaminated with signal from unconverted laser light irradiating the target aluminum-plated silicon arms; compared with using all channels we find that this effect reduces the peak intensity by approximately 100 GW sr^{-1}. An additional 105 GW sr^{-1} reduction of the peak values has been assumed as the contribution of unconverted light to the rest of the channels. These corrections are less than 2% of the peak values and do no change the error estimate significantly. However, during the early low intensity foot of the drive these corrections are proportionally much larger, resulting in an estimate for the error bar of ±10 eV. Another source of uncertainty is due to the view factor, i.e. the estimated drive of the capsule. In this study, the emission of the LEH ablated plasma has been

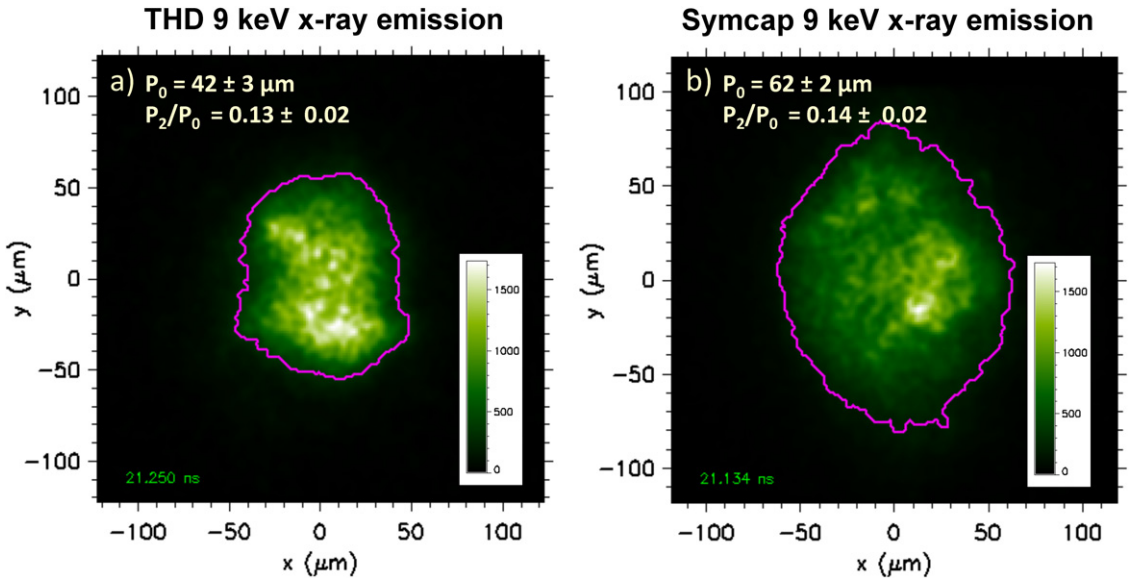

Figure 6. Comparison of the x-ray emission images at 9 keV energy from (*a*) a layered THD implosion, shot N110212, and (*b*) high-pressure gas-filled 'symcap' implosion, shot N110214. Both experiments use a 1.3 MJ laser drive and identical laser cone fractions and wavelengths. Data are shown shortly before peak x-ray emission which occurs at $t = 21.3$ ns$\pm$0.1 ns in both cases. The hohlraum axis of symmetry is vertical.

subtracted when estimating the internal radiation temperature; in future studies, to improve accuracy, additional view factor corrections may be needed due to the size of the gold plasma that is ablated from the hohlraum walls.

For seven experiments with 1 to 1.08 MJ laser energy delivered to the hohlraum, the hohlraum absorbs 870 $\pm$ 30 kJ and the radiation temperature varies from 281 to 288 eV with an absolute error bar of 5 eV. These data indicate a reproducible temperature with a standard deviation of approximately 3 eV in temperature and 4% for the radiant intensity. These results meet the requirements for the ignition point design.

In addition, at 1.3 MJ energy, symmetric implosions have been achieved. For layered THD implosions, this observation is correlated with adequate drive in the foot during the first 12 ns of the experiment. The inset in figure 5(*a*) shows that during the first 3 ns the 2 keV Dante signal is appreciably larger for the 1 MJ, 1.1 TW sr^{-1} layered THD implosion shot N100929 than for the 1.3 MJ, 1.4 TW sr^{-1} layered THD implosion shot N110212. This difference is attributed to condensates on the LEH windows for the early 1 MJ experiment. Subsequent 1.3 MJ THD implosions used storm windows, resulting in a much smaller early time 2 keV Dante signal indicating the lack of Ar emission from condensates and a total signal level consistent with expectations. This is illustrated in the Dante drive as calculated with two-dimensional radiation-hyrodynamic simulations [30] that show bright early time emission when the laser beams burn through 1 μm thick condensate. Without condensates, however, a much less intense signal from the hohlraum walls is predicted for the first 2 ns of the experiment than compared with condensates.

3.3. Implosion symmetry

At peak compression, the implosion symmetry is inferred from high-resolution (10 μm) temporally resolved (40 ps) imaging measurements of the x-ray emission from the central hot-spot plasma. These measurements can be quantified [59–61] by decomposing the soft x-ray flux asymmetry at the capsule into Legendre polynomials, P_n. Odd orders ($n = 1, 3, ...,$) are approximately zero due to the up–down illumination symmetry and low-order even modes ($n = 2, 4, ...,$) are the most important asymmetries. Higher order drive variations are negligibly small and smoothed by the hohlraum radiation environment.

Figure 6 shows the x-ray emission from the 1.3 MJ THD implosion and a comparison symcap implosion with the same hohlraum drive conditions. While THD capsules use 68 μm thick THD ice layers that contain the nuclear fuel, the symcap implosions employ a 32 μm thick plastic layer instead of a 5 μm thick layer on the inside of the Ge-doped layers; the additional mass simulates the fuel payload. The symcap capsule is shot at cryogenic temperatures of 24 K and uses a high-pressure 30% D_2, 70% ^{3}He fill at 6.32 mg cm^{-3}. The symcap implosions have been routinely used for shape measurements [3, 7, 8, 62] while the THD experiments provide additional areal density and hot-spot formation data in preparation for DT fills [19].

For the THD implosion in figure 6(*a*), the x-ray peak emission (bangtime) is at $t = 21.35 \pm 0.03$ ns, the burn width is 180 $\pm$ 40 ps with the following Legendre coefficients: $P_0 = 42\,\mu$m, $P_2/P_0 = 0.13$, $P_4/P_0 = 0.02$, $P_6/P_0 = -0.06$. The orthogonal view also indicates a fairly symmetric implosion with $M_0 = 39\,\mu$m, $M_2/M_0 = 0.07$, and $M_4/M_0 = 0.07$, and similar values for bangtime and burn width of $t = 21.39 \pm 0.03$ ns and 210 $\pm$ 40 ps, respectively. These values compare well with the symcap implosion where the x-ray peak emission is at $t = 21.35 \pm 0.03$ ns, the burn width is 186 $\pm$ 40 ps, and the following Legendre coefficients: $P_0 = 62\,\mu$m, $P_2/P_0 = 0.14$, $P_4/P_0 = 0.07$, $P_6/P_0 = -0.06$ with $M_0 = 55\,\mu$m and $M_4/M_0 = 0.042$.

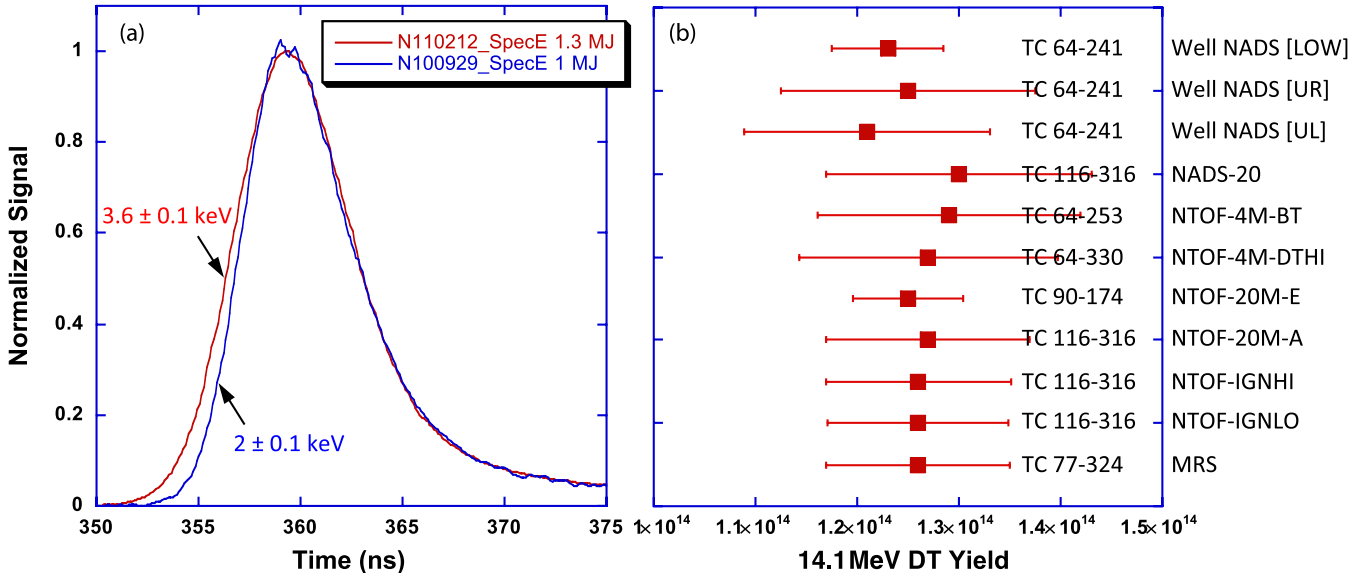

Figure 7. (*a*) Example of neutron time-of-flight data for the 1 MJ N100929 THD shot and the 1.3 MJ N110212 THD shot. The temporal data (*a*) clearly show increased thermal broadening for the high-energy implosion. (*b*) The 14.1 MeV DT yield data from 11 different NTOF, NAD, and MRS detectors at various lines of sight show excellent agreement among each other with a standard variation of 2.1%.

We have achieved symmetric implosions and adequate equatorial x-ray drive without changing the initial inner and outer cone laser powers. This tuning mechanism takes advantage of the multiple laser beam interactions with the plasma in the LEH area where all the beams cross. Transferring power into the inner beams allows us to compensate for SRS losses of the inner beams. Inner beam SRS energy losses of order 10–15% of the total energy delivered into the hohlraum are expected to affect the local soft x-ray production and drive symmetry during the peak of the laser drive.

The crossing lasers in the LEH produce spatial intensity modulations. These intensity modulations further drive plasma electron density modulations due to the ponderomotive force. If these modulations move with the plasma sound speed C_S then modulations and laser scattering will grow to large levels and efficient energy transfer between beams will occur. In the rest frame, the power transfer rate, Q, is determined by

$$Q \sim \left[(\omega_1 - \omega_2) - k_A \left(C_S - V_p\right) + i\nu\right]^{-2}. \qquad (7)$$

In equation (7), V_p is the plasma flow velocity and ν is the Landau damping rate for acoustic fluctuations. The frequency de-tuning between pairs of beams is denoted as $\omega_1 - \omega_2$. This factor allows us to control the energy transfer between cones of beams in integrated hohlraum experiments, and can be set to transfer power into either cone of beams. Proper choice of the laser wavelength difference of $\delta\lambda = 0.6$ nm (at the fundamental glass laser wavelength) for data in figure 6 has provided the desired x-ray drive symmetry.

4. Nuclear performance of layered THD implosions

4.1. Hot-spot formation

The high temperatures of ICF implosions produce brief flashes of DT or DD neutrons with thermally broadened spectral peaks. The neutron flashes spread in time as they travel to intercept neutron time-of-flight (NTOF) detectors, producing a signal pulse that provides yield (from the pulse integral), the spectral width (or burn temperature) from the pulse width, and neutron 'bangtime' from the pulse center time. Bangtime numbers indicate the time of maximum neutron yield rate, which is generally within 100 ps of maximum x-ray and gamma-ray emission. Scintillator/photodetector combinations provide high sensitivity (>10% interaction, with ≃2 ns response time, while solid state thin CVD diamond detectors (typically <1 mm) provide fast time response (<1% interaction, ≃1 ns response time). Here, interaction is the probability that a neutron passing through the detector will interact with it. Neutrons passing through thick scintillators have a higher probablity to interact, which is part of the reason for its higher sensitivity. As a general rule, NTOF detectors closest to the source record the most accurate bangtimes and yields; while the increased temporal spreading in detectors further from the source results in more accurate burn temperature measurements.

Figure 7 shows normalized NTOF data from the NTOF-20-E detector for a 1 MJ and a 1.3 MJ THD implosion. This detector is at a distance of about 22 m from target chamber center and in the equatorial plane at $\theta = 90^\circ$ and at $\phi = 174^\circ$ in spherical target chamber coordinates. The detector uses a PMT140 photomultiplier coupled to a quenched xylene liquid scintillator. We observe increased thermal broadening in going from 1 MJ to 1.3 MJ indicating a temperature increase from 2 keV to 3.6 keV. The fit to the NTOF data allows temperature measurements with an error bar of ±0.1 keV. Furthermore, the measured yield is in excellent agreement with other detectors that use different methods for determining the neutron yield. On NIF, there are a total of nine NTOF detectors at about 4–22 m distance from target chamber center. In addition, neutron activation diagnostics (NADs) and the magnetic recoil

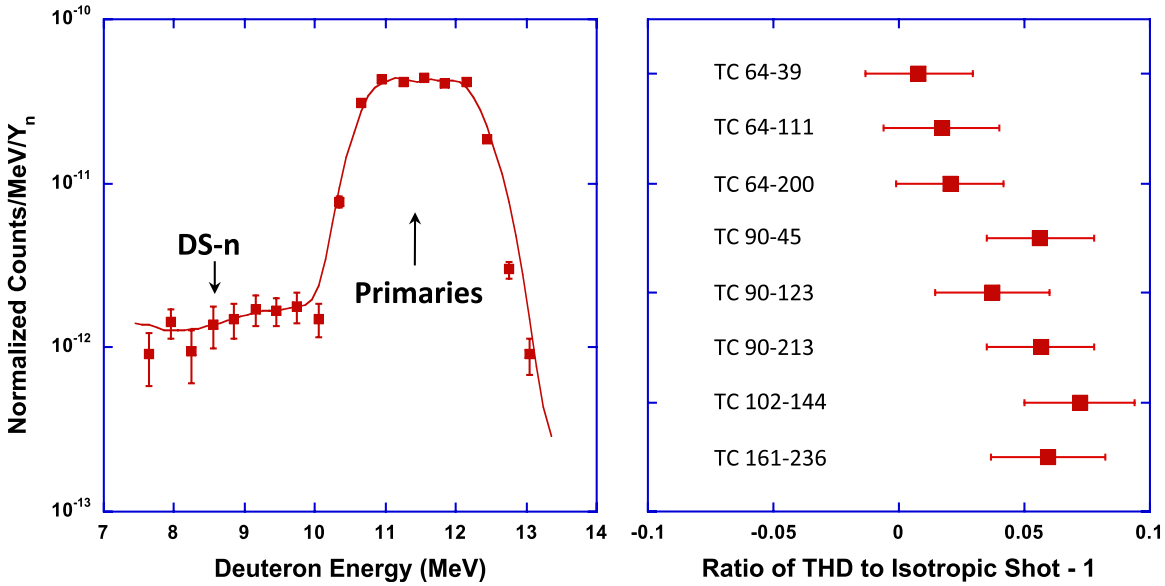

Figure 8. (*a*) Example of MRS data for 1.3 MJ THD implosion, shot N110212. The deuteron spectrum provides accurate data on the down-scattered ratio. (*b*) The 14.1 MeV DT yield data from this shot measured with 8 different NAD detectors at various line of sights and normalized to an isotropic exploding pusher experiment indicate fairly isotropic areal density.

spectrometer (MRS) [64] are employed and their locations in spherical coordinates are listed in figure 7(*b*).

Zirconium, copper and indium activation foils are used to measure DT and DD yield, ρR, and ρR anisotropies through a suite of NADs. These materials undergo neutron reactions with energy thresholds just below the DT (Zr and Cu) or DD (In) neutron production energy region of interest. The radioactive decay of the reaction product is then measured to determine the incident primary neutron fluence above the energy threshold.

The 'Well-NAD' diagnostic measures absolute 14.1 MeV DT neutron yield with three 7 cm diameter zirconium disks of 1.0, 3.5 and 8.7 mm thickness, inserted 4.5 m from the target chamber center in a diagnostic well at the (θ, ϕ) coordinates of (64,241). This location is in front of the target chamber first wall but outside the chamber vacuum, which minimizes scatter effects while allowing for easy sample retrieval. The zirconium samples undergo ^{90}Zr(n,2n) reactions with a 12 MeV threshold, producing ^{89}Zr that decays with a 3.27 day half life and emission of 909 keV gamma rays. These gamma rays are measured in a low-background counting facility with high-purity germanium detectors. Corrections to the yield due to attenuation and scatter in the 1 cm thick aluminum well assembly which holds the sample and the sample itself were calculated to be of order a few percent using MCNP [63]. The absolute DT yield is also measured using copper samples, designated 'NAD20,' in front of the NTOF20 diagnostics in the neutron alcove at (116, 316) at a distance of ~20 m from the target. The back-to-back 511 keV gamma rays from the β+ decay of ^{62}Cu are detected in coincident NaI detectors.

We find that the DT yield determined by these diagnostics are in excellent agreement with each other. The error bars for the absolute diagnostics, Well-NAD and MRS are 7% and 4%, respectively. When comparing the results from all detectors we find for these experiments that the 14.1 MeV DT yield reaches 1.3×10^{14} with a standard variation of 2.1%.

4.2. Fuel assembly

14.1 MeV DT fusion neutrons from the central hot-spot plasma lose energy by collisions in the dense fuel shell. Thus, neutrons measured in the energy range between 10 and 12 MeV probe the areal density of layered implosions. The accuracy of these measurements depends strongly on both the areal density, ρR, and the DT yield, and for these experiments we find that at DT yields above 10^{14} the down-scattered ratio of dsr = N(10–12 MeV)/N(12–15 MeV) can be determined with an error bar of less than 10%. From radiation-hydrodynamic simulations [29, 30] the areal density of the fuel is then inferred using ρR (g cm^{-2}) = 21 × dsr.

The MRS [64] has been commissioned on NIF to provide high accuracy measurements of the dsr. This diagnostic employs a carbon–deuterium (CD) foil (275 μm thick, 13 cm^2 area) at a distance of 26 cm from target chamber center and in the direction $\theta = 77^\circ$, $\phi = 324^\circ$. The DT neutrons from the implosion collide with the deuterons in the foil; the forward scattered deuterons are spectrally analyzed by a magnet at a distance of 570 cm from the foil. The DT neutrons transfer most of their momentum to the deuterons with n(14.1 MeV) + d → n′(1.6 MeV) + d(12.5 MeV). After passing the magnet, the recoil deuterons are measured with a series of CR-39 detectors and the position allows inferring their energy spectrum.

Figure 8(*a*) shows an example of the measured deuteron spectrum from the MRS for a 1.3 MJ THD implosion. While a sufficiently large number of counts for DT yields above 10^{14} results in small error bar for the total counts, the deuteron spectrum from primary and down-scattered neutrons is marginally resolved in these data. Future studies will improve the energy resolution using a medium (125 μm thick, 13 cm^2 area) or high-resolution (50 μm thick, 13 cm^2 area) CD foil which will allow $\Delta E/E = 0.05$ with the potential to observe non-thermal features in the primary neutron spectrum.

In figure 8(*a*), a 14.1 MeV fusion yield of $Y_{\rm DT} = (1.27 \pm 0.1) \times 10^{14}$, a down-scattered ratio of dsr $= (2.8 \pm 0.3)\%$ and an areal density of $\rho R = 0.56\,{\rm g\,cm^{-2}}$ were determined.

A measurement of the relative neutron yield anisotropies caused by scatter in a spatially variable areal density of the imploding capsule is provided by the 'Flange-NAD' diagnostic system. Neutrons along any particular line of sight that scatter in the dense fuel lose enough energy to drop below the 12 MeV (n,2n) activation threshold of ^{90}Zr. By observing relative differences in the activation of ~200 g zirconium samples placed on the surface of eight to ten ports around the chamber, normalized to an isotropic 'exploding pusher' shot, provide a measure of yield anisotropies; deviations as low as ~3% can be detected. To minimize systematic uncertainties, all samples are measured in the same detector using an automated positioning system. Figure 8(*b*) shows that the results are consistent with a fairly isotropic distribution within the uncertainties.

The present areal densities of $0.5\,{\rm g\,cm^{-2}}$ are higher than achieved on previous laser experiments. For example, experiments at GEKKO XII have reported $0.1\,{\rm g\,cm^{-2}}$ [65] and recent experiments at Omega have resulted in $0.3\,{\rm g\,cm^{-2}}$ [66–68]. However, the present values are a factor of three times smaller than predicted by radiation-hydrodynamic simulations for fully tuned layered implosions. For this reason, a shock timing campaign is currently underway on NIF, that is designed to tune the timing and strength of the four laser peaks that launch and set the velocity of the four shock waves that travel through the ablator and THD fuel [39, 69].

4.3. Burn duration

To estimate performance and proximity of an implosion to the ignition regime, we analyze neutron yield, the down-scattered ratio, nuclear burn duration and the burn-averaged implosion pressure from x-ray and nuclear diagnostics. Figure 9 shows the experimental traces from the gamma-ray history (GRH) detector from the 1.3 MJ THD implosion. The GRH detector [70] is located at $\theta = 64^\circ$, $\phi = 20^\circ$ and employs fast photomultipliers with a Mach–Zehnder modulator for optical transmission to measure the Cherenkov emission from high-energy gamma rays produced in the implosion experiment. Commissioning experiments with exploding pusher targets have shown that bangtime is measured with an uncertainty of ±30 ps and burn width with an uncertainty of ±15 ps.

Four cells are being fielded with two fill gases (CO_2, SF_6) and pressures to obtain signals for gamma-ray photons above 3, 5 and 10 MeV. Thus, the channels discriminate ~4 MeV γ-rays from ^{12}C and bremsstrahlung from the hohlraum and target mounting. The 10 MeV channel measures γ-rays that are produced in the DT fusion reactions, i.e. $D + T = {}^5{\rm He}^\star$ which decays with almost 100% probability to ^{4}He(3.5 MeV) + n(14.1MeV) or with a probability of 3×10^{-5} to ^{5}He + γ(16.75) MeV. For THD implosions, this signal blends with the HT_γ close to ~20 MeV. Advantages of GRH measurements are the facts that the gamma emission is isotropic and insensitive to the areal density.

The three curves in figure 9 show a 180 ps long signal from fusion gammas (DT and HT) together with the signal from the thermo-mechanical package (TMP), and further combined with the ^{12}C from the ablator. In addition to burn duration, these measurements will allow further investigations of DT implosions, where the GRH will be configured to provide an accurate measurement of yield (since the HT gamma signal will be negligible), areal density from the ablator signature, and low-energy neutrons from scattering in the fuel.

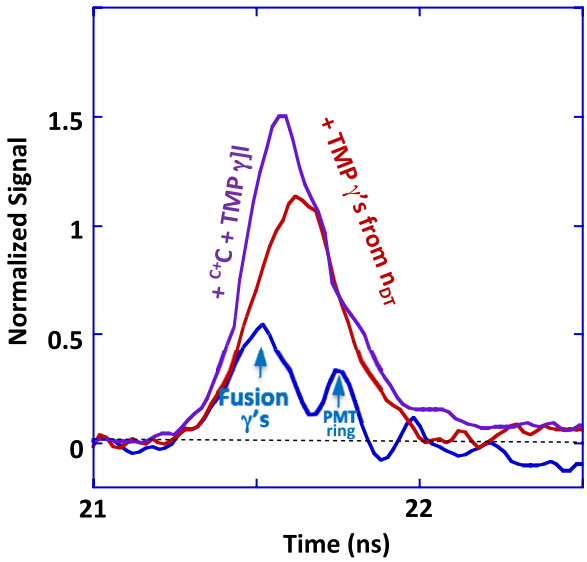

Figure 9. (*a*) Gamma-ray history signal is shown from a 1.3 MJ implosion indicating 180 ± 50 ps burn width, shot N110212. The curves reflect fusion gammas (DT and HT), combined signal from the thermo-mechanical package (TMP), and combined signal with the TMP and from ^{12}C in the ablator.

4.4. Confinement

Figure 10 shows measured DT and DD neutron yields from cryogenic layered THD and symcap implosions, respectively. The experimental data are compared with two-dimensional radiation-hydrodynamic simulations using the code HYDRA [30]. By multiplying the calculated yields with factors of 0.3 for THD and 0.5 for DD, respectively, we obtain a fairly good match between simulations and experiments. The smaller than calculated yields may be explained by the fact that the present simulations do not include surface roughness perturbations from the capsule ablator and the ice, see section 2.3. Preliminary three-dimensional calculations indicate that including physical surfaces indeed provides a factor of two to three lower yields. Future studies will need to be performed to estimate yields with realistic surfaces, and with the shape and entropy of the present experiments.

In figure 10, we observe that the 14.1 MeV yield from THD implosions follows a simple scaling that is derived from calculations of the total DT yield

$$Y_{\rm DT} = f_{\rm D} f_{\rm T} n^2 \langle \sigma_{\rm DT} v \rangle \times V \times \tau. \qquad (8)$$

Here, $\langle \sigma_{\rm DT} v \rangle$ is the DT fusion cross section averaged over the Maxwell Boltzmann velocity distribution function, $f_{\rm D}$, $f_{\rm T}$ and n are the fraction of deuterium and tritium in the plasma and the total number density of deuterium and tritium, respectively.

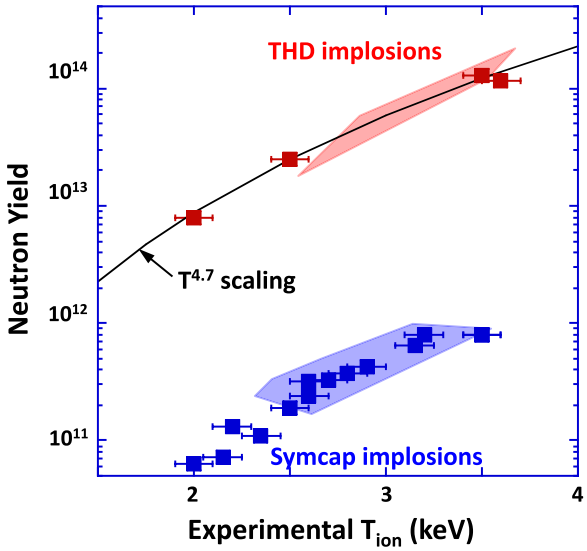

Figure 10. Burn-averaged DT and DD neutron yields are shown for cryogenic layered THD implosions and high-pressure D ^{3}He gas-filled symcap implosions. The DT yield follows the expected $T^{4.7}$-scaling with temperature and compare well with two-dimensional radiation-hydrodynamic simulations that are multiplied by 0.3 for THD (red area) and 0.5 for DD symcaps (blue area).

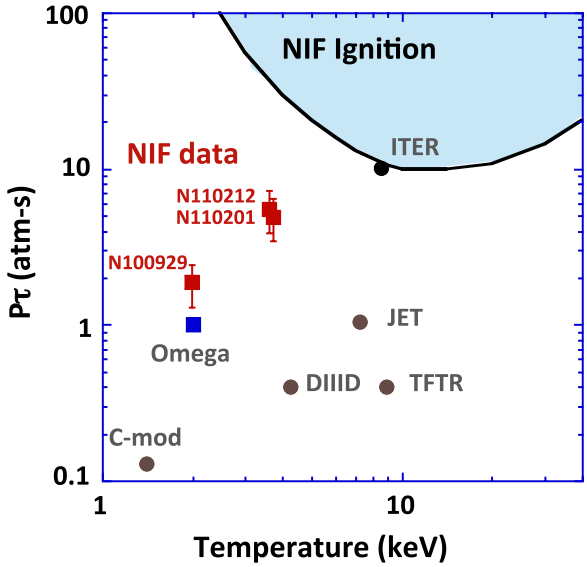

Figure 11. Generalized Lawson confinement parameter, averaged pressure times confinement time, $P\tau$, versus the ion temperature is shown. The figure compares finding from NIF implosions, Omega laser data, and various tokamak results. The data indicate that these first cryogenic layered implosions reach high confinement parameters. For ignition, the implosions will need to be further improved to achieve higher values for $P\tau$ with pressures above 300 Gbar.

V is the hot-spot volume and τ is the burn duration. The $T^{4.7}$-scaling is primarily a consequence of the cross section scaling with temperature for the present experiments; volume, burn duration and hydrogen isotope ratios are set constant. This result implies no major difference in mix [71] among these THD experiments which is currently being investigated with detailed measurements of the x-ray emission spectra from ablator dopants [72].

The neutron yield and down-scattered ratios can be combined into an experimental ignition threshold factor (ITFx) [73]. For an equivalent DT-implosion, the ITFx-value is defined as

$$\mathrm{ITFx} = \left(\frac{Y_n}{3.2 \times 10^{15}}\right)\left(\frac{\mathrm{dsr}}{0.07}\right)^{2.3}. \qquad (9)$$

This formalism allows the direct use of accurately measured quantities for estimating the proximity toward the ignition regime for inertial confinement fusion experiments. In this study, we use THD with $f_\mathrm{D} = 0.06$ and $f_\mathrm{T} = 0.72$. To obtain the no-alpha particle self-heating DT equivalent yield, Y_n, we scale the measured 14.1 MeV Y_DT data according to equation (8) with $(0.5^2)/(0.06 \times 0.72) \simeq 5.8$ and obtain ITFx $\simeq 0.02$.

THD implosions allow approaching the threshold ITFx values for alpha heating and ignition in controlled well-diagnosed experiments. For example, THD fuel with a deuterium fraction as low as 2% will allow measurements of threshold conditions at neutron yields of about $Y_\mathrm{DT} \sim 3.2 \times 10^{15} \times ((0.02 \times 0.74)/(0.5 \times 0.5)) = 2 \times 10^{14}$ where alpha particle heating will not play a role. A series of about 1000 two-dimensional simulations with and without alpha heating has been performed to assess the surrogacy of the THD platform for determining the threshold for inertial confinement fusion [14, 73]. The simulations indicate that the higher THD vapor pressures produce different particle densities in the central gas cavity compared with the DT (the fuel mass density has been chosen to be constant). THD implosions with 6% deuterium at 17.4 K provide particle densities of 2.9×10^{-4} mol cm^{-3}, significantly larger than DT implosions at 18 K with 1.1×10^{-4} mol cm^{-3}. This effect results in about 10% lower temperatures in THD implosions compared with DT. Nevertheless, the simulations show that THD implosions with ITFx values of about 1 (1.2) show a 50% (90%) probability for ignition and fusion yield of 20 MJ when fielding the experiment with DT fuel.

With the volume determined from x-ray emission images, the density obtained from x-ray or neutron yield, burn duration from GRH, and temperatures from the NTOF we can determine the pressure and the Lawson confinement parameter. For these experiments, we find that the pressure increases from 9 Gbar at 1 MJ to 30 Gbar for the 1.3 MJ layered THD implosion. Combined with the burn duration we find 1.8 atm × s and 6 atm × s.

Figure 11 shows the pressure–time product versus the measured ion temperature for NIF implosion shots. Radiation-hydrodynamic simulations indicate that ignition conditions will be reached at $P\tau \simeq 30$ and no-alpha particle heating temperatures of $T = 4$ keV. The values achieved in this study are determined from averaged pressure data and well exceed the results quoted from previous fusion experiments [17] including Omega [68] and various tokamaks. The latter include results from DIIID [74, 75] and JET [76, 77] and have achieved values of order 1 atm × s in both cases.

Future experiments are being planned to further tune the implosions to reach values of about 30 atm × s which are

predicted for the ignition regime. The next tuning steps will include improvements in shock timing to lower the entropy and increase the fuel areal density and pressure. Also, the implosion velocity and shape will be further optimized by varying the hohlraum dimensions, by increasing the laser power, and by modifying the capsule ablator.

5. Conclusions

We have performed the first implosion experiments with thermonuclear cryogenic fuel on the National Ignition Facility. These experiments are driven by radiation temperatures of 300 eV produced by 1.3 MJ laser energy delivered by 192 ultraviolet laser beams. An extensive suite of optical, x-ray and nuclear diagnostics has demonstrated accurate measurements of important implosion performance parameters. In particular, we find that these first implosions compress to a spherical dense fuel shell of about 0.5 g cm^{-2} that contains a 80 μm diameter hot plasma core at temperatures of 3.5 keV which produces a DT neutron yield in excess of 10^{14} 14.1 MeV neutrons. These first layered experiments have shown high areal densities and high Lawson confinement parameters. These implosions provide the experimental platform for investigating mix, velocity, entropy and shape in preparation for fielding DT implosions with high probability for ignition and thermonuclear burn.

Acknowledgments

This work was performed under the auspices of the US Department of Energy by Lawrence Livermore National Laboratory under Contract DE-AC52-07NA27344. This work was also supported by the US Department of Energy Office of Inertial Confinement Fusion under Cooperative Agreement No DE-FC52-08NA28302.

References

[1] Moses E I and Wuest C R 2005 *Fusion Sci. Technol.* **47** 314
[2] Haynam C *et al* 2007 *Appl. Opt.* **46** 3276
[3] Glenzer S H *et al* 2010 *Science* **327** 1228
[4] Michel P *et al* 2010 *Phys. Plasmas* **17** 056305
[5] Meezan N B *et al* 2010 *Phys. Plasmas* **17** 056304
[6] Kline J L *et al* 2011 *Phys. Rev. Lett.* **106** 085003
[7] Glenzer S H *et al* 2011 *Phys. Rev. Lett.* **106** 085004
[8] Town R P J *et al* 2011 *Phys. Plasmas* **18** 056302
[9] Lindl J D *et al* 1995 *Phys. Plasmas* **2** 3933
[10] Lindl J D *et al* 2004 *Phys. Plasmas* **11** 339
[11] Landen O L *et al* 2011 *Phys. Plasmas* **18** 051002
[12] Haan S W *et al* 2011 *Phys. Plasmas* **18** 051001
[13] Moses E I 2011 *Fusion Sci. Technol.* **60** 11
[14] Spears B K *et al* 2010 *J. Phys. Conf. Ser.* **244** 022014
[15] Chang Py *et al* 2010 *Phys. Rev. Lett.* **104** 135002
[16] Lawson J D 1957 *Proc. Phys. Soc.* B **70** 6
[17] Betti R *et al* 2010 *Phys. Plasmas* **17** 058102
[18] Zhou C D and Betti R 2008 *Phys. Plasmas* **15** 102707
Zhou C D and Betti R 2009 *Phys. Plasmas* **16** 079905
[19] Edwards M J *et al* 2011 *Phys. Plasmas* **18** 051003
[20] Haan S W *et al* 1995 *Phys. Plasmas* **2** 2480
[21] Atzeni S and Meyer-ter-Vehn J 2004 *The Physics of Inertial Fusion* (New York: Oxford University Press)
[22] Kucheyev S O and Hamza A V 2010 *J. Appl. Phys.* **108** 091101
[23] Michel P *et al* 2009 *Phys. Rev. Lett.* **102** 025004
[24] Clark D S, Haan S W and Salmonson J D 2008 *Phys. Plasmas* **15** 056305
[25] Robey H 2012 *Phys. Plasmas* submitted
[26] Miller J R 1975 *Los Alamos Scientific Laboratory Report* LA-6245-PR, p 82
Miller J R 1987 Methods and Apparatusfor Producing Cryogenic Inertially Driven Fusion Targets (*US Patent*) 4,292,340 (January 1987)
[27] Martin A J, Simms R J and Musinski D L 1988 *Sci. Technol.* A **6** 1885
[28] Hoffer J K and Foreman L R 1988 *Phys. Rev. Lett.* **60** 1310
[29] Zimmerman G B and Kruer W L 1975 *Comment. Plasma Phys. Control. Fusion* **2** 85
[30] Marinak M M *et al* 2001 *Phys. Plasmas* **8** 2275
[31] MacGowan B J *et al* 1996 *Phys. Plasmas* **3** 2029
[32] Glenzer S H *et al* 2007 *Nature Phys.* **3** 716
[33] Lefebvre E *et al* 1998 *Phys. Plasmas* **5** 2701
[34] Moody J D *et al* 2001 *Phys. Rev. Lett.* **86** 2810
[35] Kato Y *et al* 1984 *Phys. Rev. Lett.* **53** 1057
[36] Berger R L *et al* 1998 *Phys. Plasmas* **5** 4337
[37] Dewald E L *et al* 2011 *Phys. Plasmas* **18** 092703
[38] Celliers P 2012 *Phys. Plasmas* submitted
[39] Robey H 2012 *Phys. Rev. Lett.* submitted
[40] Boehly T R *et al* 2011 *Phys. Plasmas* **18** 092706
[41] Offenberger A A *et al* 1982 *Phys. Rev. Lett.* **49** 371
[42] Drake R P *et al* 1984 *Phys. Rev. Lett.* **53** 1739
[43] Moody J D *et al* 2010 *Rev. Sci. Instrum.* **81** 10D921
[44] Glenzer S H *et al* 1998 *Phys. Rev. Lett.* **81** 365
[45] Regan S *et al* 2010 *Phys. Plasmas* **17** 020703
[46] Kilkenny J D *et al* 1995 *Rev. Sci. Instrum.* **66** 288
[47] Doeppner T 2012 *Phys. Rev. Lett.* at press
[48] Michel P *et al* 2009 *Phys. Plasmas* **16** 042702
[49] Michel P *et al* 2011 *Phys. Rev.* E **83** 046409
[50] Dewald E L *et al* 2004 *Rev. Sci. Instrum.* **75** 3759
[51] Dewald E L *et al* 2005 *Plasma Phys. Control. Fusion* **47** 405
[52] Schneider M B *et al* 2010 *Rev. Sci. Instrum.* **81** 10E538
[53] Meezan N I *et al* 2011 *Inertial Fusion Science Application Conf. (Bordeaux, France)*
[54] Dattolo E *et al* 2001 *Phys. Plasmas* **8** 260
[55] Marshak R E 1958 *Phys. Fluids* **1** 24
[56] Suter L J *et al* 1994 *Phys. Rev. Lett.* **73** 2328
[57] Glenzer S H *et al* 1998 *Phys. Rev. Lett.* **80** 2845
[58] Sigel R *et al* 1990 *Phys. Rev. Lett.* **65** 587
[59] Hauer A A *et al* 1995 *Phys. Plasmas* **2** 2488
[60] Landen O L *et al* 1999 *Phys. Plasmas* **6** 2488
[61] Turner R E *et al* 2000 *Phys. Plasmas* **7** 333
[62] Kyralla G A *et al* 2011 *Phys. Plasmas* **18** 056307
[63] Briesmeister J F 1997 MCNP—A General Monte Carlo N-Particle Transport Code, Version 4B, Los Alamos National Laboratory
[64] Frenje J A *et al* 2010 *Phys. Plasmas* **17** 056311
[65] Azechi *et al* 1991 *Laser and Part. Beams* **9** 193–207
[66] Betti R *et al* 2006 *Plasma Phys. Control. Fusion* **48** B153–63
[67] Goncharov *et al* 2010 *Phy. Rev. Lett.* **104** 165001
[68] Sangster *et al* 2008 *Phy. Rev. Lett.* **100** 185006
[69] MacKinnon A J *et al* 2012 *Phy. Rev. Lett.* at press
[70] Herrmann H W *et al* 2010 *Rev. Sci. Instrum.* **81** 10D333
[71] Hammel B A *et al* 2011 *Phys. Plasmas* **18** 056310
[72] Regan S 2012 *Phys. Rev. Lett.* submitted
[73] Spears B K *et al* 2012 *Phys. Plasmas* at press
[74] Lazarus E A *et al* 1996 *Phys. Rev. Lett.* **77** 2714
[75] Lazarus E A *et al* 1997 *Nucl. Fusion* **37** 7
[76] Keilhacker M *et al* 1999 *Plasma Phys. Control. Fusion* **41** B1–23
[77] Keilhacker M *et al* 1999 *Nucl. Fusion* **39** 209